Self-Adjustable Step-Based Control Algorithm for Grid-Interactive Multifunctional Single-Phase PV-Battery System Under Abnormal Grid Conditions

Shailendra Kumar, *Member, IEEE*, Laxmi Narayan Patel, Bhim Singh, *Fellow, IEEE*, and A. L. Vyas

***Abstract*—This article deals with the single-phase grid interactive multifunctional solar PV (photovoltaic) system with seamless power transfer capability. This multifunctional PV-battery system is also helpful to enhance the quality of power in the utility grid. The system provides an uninterrupted power to nonlinear loads during the nonavailability of utility and renewable energy resource. This PV-battery system comprises two stages. First stage is a PV array-boost converter along with a battery energy storage-bidirectional converter that is integrated at dc-link and another is voltage source converter (VSC), which performs the task of harmonics elimination and injection of harvested energy to the utility along with nonactive power compensation. In standalone mode, the shape of load voltage is sustained sinusoidal by islanded technique. A proportional integral controller is used to sustain the dc-link voltage to a specific value. In order to improve the dynamic response of the PV-battery system, a feedforward control for solar PV participation is used. A self-adjustable step-based control is introduced for the VSC in this work. This estimates the real power reflecting portion of the load current in order to show the features of the PV-battery system. Simulation studies are carried out in MATLAB Simulink. The experimental performance of the developed PV-battery system is found satisfactory even under abnormal grid condition.**

***Index Terms*—MPPT, power quality, PV, sag, swell, VSC.**

I. Introduction

NONCONVENTIONAL energy sources such as solar energy is clean, green, and free source of energy. The other advantages of the solar energy are that it does not produce the greenhouse effect and it is present in nature abundantly. So, the photovoltaic (PV) system becomes popular due to easy installation and less maintenance. Moreover, the cost-effective topology is a major concern for the good design engineers. The PV-battery system is becoming popular because it is reaching parity to the grid [1], [2]. However, under loss of the distribution network, grid-connected solar systems are necessary to shut down because of protection reasons. Therefore, for supplying uninterrupted energy to the emergency load and for peak power saving, a utility interactive PV-battery system with energy storage is an attractive solution [3], [4]. Here, a battery storage also provides the smoothing facilities to the intermittent PV generation. Moreover, a bidirectional power converter is an essential component to control the operation of the battery storage in both the modes.

Solar energy produced by PV cell depends on the irradiance and temperature. Both quantities are variable; also, the V–I curve of the PV array is nonlinear in atmosphere. Therefore, in order to extract the crest energy from a PV array, there is only single point on power vs. voltage curve. This operating point can be varying depending upon the climate conditions. So, the researchers have investigated several algorithms for maximum power point tracking (MPPT). The MPPT controllers for grid-connected PV array have been reviewed in [3]. The perturb and observe MPPT technique with variable step size for standalone PV system is introduced in [4]. The MPPT method based on change in conductance is introduced in [5]. An incremental conductance method is used, in this article, because it is easy and simple to implement and it also results in good performance under varying insolation.

For many purposes, grid-connected voltage source converters (VSCs) are used. Several VSC-based topologies for grid-connected systems are presented in [6]. Distribution static synchronous compensators (D-STATCOMs) and active power filters built with VSC are introduced by researchers. D-STATCOM comprises current-controlled VSC, which feeds current at point of common coupling (PCC) through the inductor. The operation of VSC is accomplished with the help of dc-link capacitor with specific voltage across it. VSC is treated as shunt-connected device in many applications. There are many control algorithms available for the D-STATCOM. Compensations based on current error for VSC current control in weak grid for wind farm applications are presented in [7]. A control method, which uses second-order generalized integrator, is presented in [8]. Many researchers have shown that the grid-connected PV-battery system is used for other purposes rather than only feeding power to the

Manuscript received November 17, 2019; accepted February 22, 2020. Date of publication March 16, 2020; date of current version April 24, 2020. Paper 2019-SECSC-0504, presented at the 2018 IEEE International Conference on Power Electronics, Drives and Energy Systems, Chennai, India, and approved for publication in the IEEE TRANSACTIONS ON INDUSTRY APPLICATIONS by the Renewable and Sustainable Energy Conversion Systems Committee of the IEEE Industry Applications Society. The work was supported by the DST, Government of India under Projects RP03391G and RP03357G. *(Corresponding author: Shailendra Kumar.)*

Shailendra Kumar is with the Department of Electrical Engineering, S. V. National Institute of Technology, Surat, Gujarat-395007, India (e-mail: er.dwivedi88@gmail.com).

Laxmi Narayan Patel, Bhim Singh, and A. L. Vyas are with the Indian Institute of Technology Delhi, New Delhi 110016, India (e-mail: lnpatel91@gmail.com; bsingh@ee.iitd.ac.in; alvyas@iddc.iitd.ac.in).

Color versions of one or more of the figures in this article are available online at http://ieeexplore.ieee.org.

Digital Object Identifier 10.1109/TIA.2020.2981437

grid like reactive power compensation, maintaining the dc-link voltage. The dc-link voltage control and reactive power compensation using fuzzy-PI (proportional integral) controller in the grid-interfaced solar PV-battery system with D-STATCOM capability are presented in [9]. Harmonic elimination based on lattice wave digital filter in grid solar PV system is presented in [10]. The high-precision quadrature control for three-phase single-stage grid-connected PV-battery system is presented in [11]. Seamless transition of single-phase utility interactive PV-battery system between standalone and grid-interfaced modes is presented in [12]. The power quality features of various topologies of grid converter are presented in [13]. To reduce the burden from PI controller caused by changing the load and for providing load compensation, feedforward term is used in control so that there is minimum overshoot in the dc-link voltage. The literature, which has used digital filter-based method for active filtering, is presented in [14]. Adaptive harmonic detecting with variable step size approach applied to active power filters is presented in [15]. In this work, self-adjustable step control technique is applied for utility-tied PV-battery system. The control technique gives a separate estimation of load current, losses, and PV power participation. The unpredicted change in insolation level is controlled by feedforward control taken into account real power variation from a PV array, which reduces the burden from a PI controller. The nonideal grid condition is considered in this work. A wide range of results are obtained for abnormal grid conditions, changes in the load, and climatic condition. In this work, performance of PV-battery system is found satisfactory.

Under injection of extracted PV energy to the utility grid, the grid interactive PV-battery system must furnish a stable, sinusoidal ac voltage matches with utility voltage and frequency in accordance to the IEEE 1547 [16]. Therefore, a compact reliable and tight synchronization scheme is required. However, poor synchronization schemes lead to damage of sensitive loads, instability and many times disappearance of distribution network itself. In last decades, the phase-locked loop (PLL) provides mechanism for synchronization of VSC to the utility grid due to their robustness and tracking ability [17], [18]. Synchronous reference frame (SRF)-PLL is quite robust and calculates the phase angle at high speed if the system is purely sinusoidal [19]. However, under wide variation and harmonics present in the input signal, these techniques experience large variation in the extracted signal [20]. In order to achieve enhanced performance under distorted conditions, the PLL uses either pre-filter or in-loop filter. Under voltage distortion condition, single-phase SRF-PLL is quite sensitive to harmonics and synchronization with grid voltage, which also affects the estimated phase and frequency of distribution network. Therefore, in this article, a third-order sinusoidal integrator (SSI)-based control approach [21] is utilized to assess the angle and frequency adaptability of distribution network and to eliminate dc offset error. The third-order SSI-based approach with variable learning control improves the inherent disturbance rejection capacity of PLL.

The grid interactive system also operates during the grid failure. Therefore, to desynchronize the system from the grid during the fault, a robust and simple islanding detection scheme is required [22]. Many researches have reported the issues of islanding detection [23]. In the last few years, a communication-based islanding, active and passive methods and hybrid methods are investigated. These methods have their own merit and demerits, for example, communication-based methods, which cover most of the nondetection zone (NDZ) but because of extra communication device, this method is costly. However, passive islanding technique has large NDZ as compared to communication but it does not require any communication device. In this article, the NDZ is very small and the system rating is also small so there is no extra need of communication device for the islanding detection. Therefore, a simple passive islanding detection technique based on measurement of grid voltage magnitude, phase, and frequency is used. The outcome and benefits of PV-battery microgrid are described as follows.

1) Here, a simple, seamless transfer passive detection technique is used, which requires only information of grid voltage, angle, and frequency, and does not require any additional telecommunication device for detection of islanding. The operational cost is low and smooth transfer also protects loads from severe faults at transitions.
2) The system is controlled even under change in grid parameters at appearance and disappearance of the distribution network and polluted utility scenarios. The PLL is inherently sensitive to the disturbance and noise and has low tracking accuracy under dynamic and polluted conditions. The mode transfer control along with third-order SSI-based approach resolves the limitation of standard PLL. In PLL, frequency and synchronizing signals are not determined in dual loop. Therefore, it is realized that at the variation of input grid voltages, the functioning of the PLL becomes poor as compared to third-order SSI. The third-order SSI control remains stable even at low loop gains as it has dual loop.
3) In utility interactive mode, dc–ac converter of the system performs as a compensator unit to mitigate higher order harmonics frequency of the load and supply necessary reactive power. In addition, at unavailability of grid, the structure of load voltage is sustained by islanded algorithm to transfer the energy to loads efficiently.
4) The transfer of control algorithms from grid-interactive to standalone and re-connection is acquired without any instability and interruption in load voltages. The operation is very difficult at nonlinear unbalanced load condition as the magnitude of voltage and the frequency of it vary and prevent from damage of residential loads.

II. System Structure

The grid-interactive multifunctional PV-battery system is illustrated in Fig. 1. This system comprises four major parts. The first one is solar energy conversion system (SECS) consisting of two stages, a boost converter and a VSC. The second one is a battery storage with a bidirectional converter. The third one is load coupled at PCC and the fourth major part is a single-phase distribution grid. It consists of an interfacing inductor and a ripple filter. In order to make PV array of 4 kW rating,

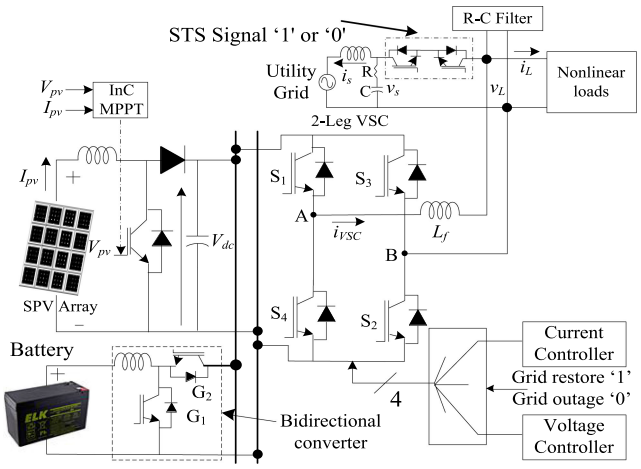

Fig. 1. System structure of PV-battery-based grid interactive system.

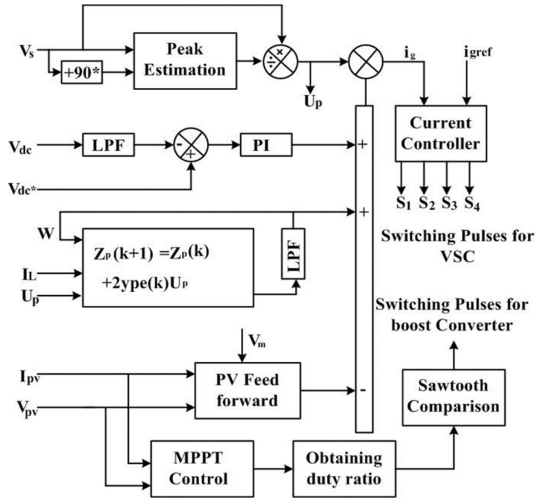

Fig. 2. VSC control in grid-tied mode.

series- and parallel-connected PV panels are used. To obtain the crest power from a PV array, MPPT control is used with a boost converter. The boost converter output is given to the dc-link of VSC. Extracted solar PV energy is given to the grid by the VSC of PV-battery system that also improves the quality of power at single-phase utility network. A full-bridge VSC having four switches (IGBT) with interfacing inductor is tied to the single-phase utility. Although to reduce the switching ripples in PCC voltage, an R-C filter is tied at PCC. The use of a battery storage suppresses the fluctation in output power of the PV array and supports the distribution netwrok at peak load demand hours. Under outage of utiltiy grid and low or zero power generation from the PV array, it supplies the energy to meet the emergency load demand. For import/export power to/from the grid, a back-to-back static transfer switch (STS) arrangment is used. The opening and closing of these switches are decided by availability of the main grid.

III. Control Approaches

The behavior of PV-battery system depends upon the control approaches. The control strategies include the adjustable step-based technique to control the system in current control mode, islanded algorithm, bidirectional dc–dc converter-controlled battery and synchronizing controller with passive islanding detection technique for shifting the control from adjustable step based technique to voltage control mode. The current control technique is presented in Fig. 2. The parameters which are sensed are PV array voltage (V_{pv}) and current (I_{pv}), dc-link voltage $(V_{\rm dc})$, load current (i_L), grid voltage (v_g), and current (i_g). Hence, total six parameters are sensed for control and feedback. One can categorize this overall control algorithm into two sections. The first one is control for a boost converter, which determines the duty cycle in which a boost converter operates to perform the MPPT function. Maximum obtained power from a solar PV array is given to the dc-link of VSC that injects the power to the utility grid. The system injects the extracted power into the grid along with improvement in the quality of power in single-phase grid, hence the system is said multifunctional. The grid current remains sinusoidal with unity power factor (UPF) irrespective of the load condition. All the reactive and harmonics currents demanded by the load are given by the VSC that is allowed by the introduced control algorithm. However, the estimation of duty cycle of battery converter is carried out for different charging and discharging scenarios.

A. Control for VSC in Grid-Interactive Mode

The VSC, which is a second stage of SECS, is an important part because it performs the tasks like injection of solar PV power into the grid, compensation of reactive power, rejection of harmonics of current, and power factor enhancement to unity. In order to achieve these tasks, the current of VSC is controlled. The introduced control technique works on the principle of balancing the real power component of distinct component of currents involved at PCC. The detailed explanation of the self-adjustable step-based control algorithm is given here.

To extract the synchronization signal (u_p), the PCC voltage is sensed. Synchronization signal is sinusoidal in nature with unity magnitude and the same phase as PCC voltage. To obtain the synchronization template, estimation of the peak of the PCC voltage is necessary, which is given by

$$V_p = \sqrt{v_\alpha^2 + v_\beta^2} \tag{1}$$

where V_p is the peak value of voltage at PCC, v_α is the grid voltage, v_β is the 90-degree phase advanced grid voltage. This peak value of the PCC voltage is used to obtain the synchronization signal, which is given as

$$u_p = v_\alpha / V_p. \tag{2}$$

A self-adjustable step-based control is used to obtain the peak load current. In the introduced control, only one neuron is used for this system. The governing equation is as [24], [25]

$$Z_p\,(k+1) = Z_p\,(k) + 2\gamma_p e\,(k)\,u_p \tag{3}$$

where γ_p is the phase neuron learning rate. One can keep this phase neuron leaning rate adjustable. The equations for

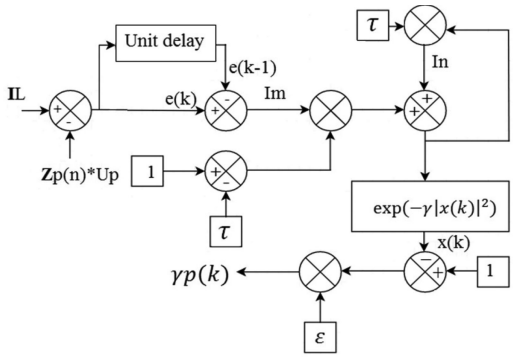

Fig. 3. Self-adjustable step-based control to extract peak load current.

maintaining the adjustable learning rate is given as

$$\gamma_p(k) = \varepsilon\left(1 - \exp\left\{1 - \rho|x(k)|^2\right\}\right) \tag{4}$$

$$x(k) = \tau x(k-1) + (1-\tau)\{e(k) - e(k-1)\}. \tag{5}$$

The difference between sensed and estimated output is given as $e(k)$ and $e(k-1)$. The constants are ε, τ, ρ, which are chosen as 0.55, 0.45, and 0.8, respectively [24]. Full algorithm is demonstrated in Fig. 3. According to the load current, γ_p is adjusted.

The PV power participation is combined for reference grid current generation and this is obtained as

$$I_{pvff} = I_{pvg} = 2P_{pv}/V_p. \tag{6}$$

If one considers the system to be lossless, then I_{pvg} is the peak value of the grid current at that time, and the load is compensated and consumes no real power. Now to fix the dc-link voltage, a PI controller is used. The loss portion of VSC is the output of the PI controller, which is calculated as

$$I_{\text{loss}}(n) = I_{\text{loss}}(n-1) + K_p\{V_{\text{dc}}(n) - V_{\text{dc}}(n-1)\} + K_i V_{\text{dc}}(n). \tag{7}$$

The peak value of the grid reference current is achieved by combining the losses, real load power, and PV power participation, which is given as

$$I_{gp} = I_{Lp} + I_{\text{loss}} - I_{pvg}. \tag{8}$$

The synchronization signal that is extracted earlier from PCC voltage is multiplied with the peak value of the reference grid current to obtain the instantaneous grid current. The current controller accepts the sensed grid current and this reference grid current accordingly generates the gating pulses for VSC.

B. Control for VSC in Islanded Mode

Fig. 4 shows the control approach for single-phase VSC based on the $\alpha\beta$ to *dq* transformation. An orthogonal component of load voltage is generated by using in-phase, which is equal to the quarter cycle delay of the load voltage and it is considered as the β component. The obtained *dq* voltage components are compared with the reference *dq* components to generate the voltage error for the PI controllers. The output of the PI controller is considered as *dq* components of the VSC current and further

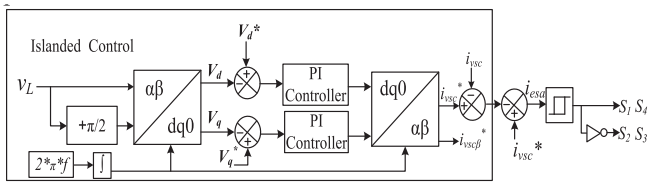

Fig. 4. Control approach for single-phase VSC.

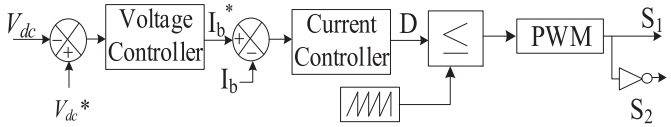

Fig. 5. Battery controller.

these are converter into $\alpha\beta$ components. The transformation from $\alpha\beta$ *to dq* and *dq* to $\alpha\beta$ is given as

$$\begin{bmatrix} v_{L\alpha} \\ v_{L\beta} \\ 0 \end{bmatrix} = \begin{bmatrix} \cos\omega t & -\sin\omega t & 0 \\ \sin\omega t & \cos\omega t & 0 \\ 0 & 0 & 1 \end{bmatrix} \begin{bmatrix} v_{Ld} \\ v_{Lq} \\ 0 \end{bmatrix} \tag{9}$$

$$\begin{bmatrix} i_{Ld} \\ i_{Lq} \\ 0 \end{bmatrix} = \begin{bmatrix} \cos\omega t & \sin\omega t & 0 \\ -\sin\omega t & \cos\omega t & 0 \\ 0 & 0 & 1 \end{bmatrix} \begin{bmatrix} i_{vsc\alpha} \\ i_{vsc\beta} \\ 0 \end{bmatrix}. \tag{10}$$

The in-phase component $(i_{\text{vsc}\alpha})$ is compared with the sensed VSC current to generate the switching pulses for the single-phase VSC.

C. Control of Battery Storage

For the battery storage control, the reference dc-link voltage is compared with the sensed dc-link voltage and given to the PI controller for estimation of battery reference current as shown in Fig. 5. The $I_{\text{batt}}*$ is compared with the sensed battery current (I_{batt}) and the output is given to PI current controller to estimate pulses for the bidirectional converter as

$$D(n+1) = D(n) + k_{pi}\{I_{\text{berr}}(n+1) - I_{\text{berr}}(n)\} + k_{ii} I_{\text{berr}}(n+1) \tag{11}$$

where *D* is the duty ratio, I_{berr} is the battery current error, and K_{pi} and k_{ii} are the gains of PI controller.

At outage of PV source and utility, a drop-off in the dc-link voltage takes place. The converter is controlled in boost mode and enabling the power flow from the battery to the dc-link and to supply power to the dedicated loads, thus discharges the battery. When the PV power is available, and the grid outage is there, then the dc-link voltage rises. Now the converter is operating in buck mode, and enabling the power flow from dc-link to the battery, thus, charges the battery. The control of the battery is also managed in the grid-connected mode under outage of a PV array. When the battery state of charge (SOC) is less than a defined value ($\leq$90%), then the current controller injects the current to the battery, generally when the unit cost of the energy is low. However, under outage of a PV array and the grid, there

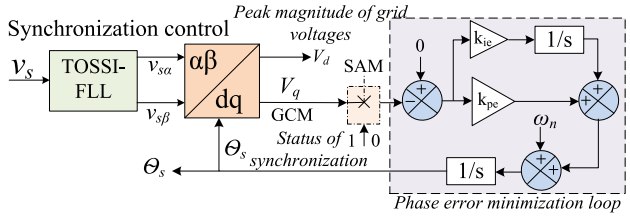

Fig. 6. Third-order SSI-FLL-based control for phase and frequency estimation.

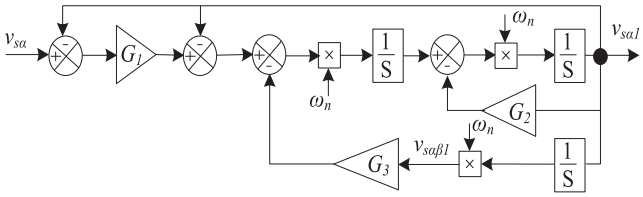

Fig. 7. Block diagram of third-order SSI.

is a decrease in the DC link voltage, so the discharging of the battery happens and the battery supplies energy to the load.

D. Synchronization and De-Synchronization With Third-Order Sinusoidal Integrator

The evaluation of phase and frequency for the synchronization is achieved through the third-order SSI-based technique. The in-phase and quadrature components of grid voltage are also extracted using the third-order SSI and converted into the stationary reference frame. The estimated frequency and angle errors are minimized through the PI controller as shown in Fig. 6.

The block diagram of third-order SSI control is shown in Fig. 7 in order to estimate the fundamental grid voltage, frequency, and phase angle. The mathematical expression of third-order SSI is estimated using the Mason's gain formula as [21]

$$T_f(s) = \frac{v_{s\alpha 1}(s)}{V_{s\alpha}(s)} = \frac{F_p}{1 - \left(\sum_{L=1}^{\text{no.of loop}} F_L\right)} \tag{12}$$

where F_p is the forward path and F_L is the number of loops. The total four loops are in the SSI control. Therefore, forward path and loop gains are estimated as [21]

$$F_p = \frac{G_1\omega_n^2}{s^2} \text{and} \left(\sum_{L=1}^{4} F_L\right) = F_1 + F_2 + F_3 + F_4 \tag{13}$$

where the values of loop paths are given as

$$F_1 = \frac{-G_1\omega_n^2}{s^2} F_2 = \frac{-\omega_n^2}{s^2} F_3 = \frac{-G_2\omega_n^2}{s^3} F_4 = \frac{-G_2\omega_n}{s}. \tag{14}$$

Using the above equations, the transfer function is derived as

$$T_f(s) = \frac{v_{s\alpha 1}(s)}{V_{s\alpha}(s)} = \frac{G_1\omega_n^2 s}{S^3 + G_2\omega_n s^2 + (G_1+1)\omega_n^2 s + G_2\omega_n^3} \tag{15}$$

where ω_n is the natural frequency and G_1 and G_2 are positive gains of the controller. The value of G_1 is selected less than 2 and then the value of G_2 is tuned to get good steady-state

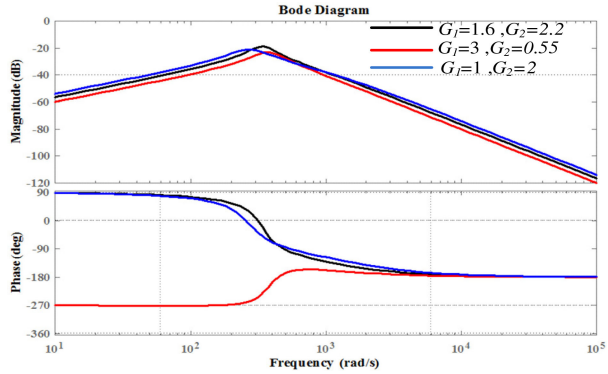

Fig. 8. Frequency plot of third-order SSI control with various value of gains.

and dynamic responses. Here, frequency analysis is performed by using various value of controller's gains, which is shown in Fig. 8. If the gains are beyond the selected value, the filter response becomes poor. The stability of the system is good in case of G1 = 1.6 and G2 = 2.2. However, for other values, the system deviates from its path and have more dc offset and phase shift between the estimated fundamental voltage and input to the SSI-based control.

IV. Simulation Results

The PV-battery-based microgrid with a bidirectional converter-controlled battery is first developed in MATLAB/Simulink and adjustable step-adaptive filter is utilized for the developed microgrid. The performance of microgrid at grid fault and recovery conditions, reactive power compensation, and improvement of dynamic response of the system, are presented in this section. A diode bridge rectifier with a resistance and inductance is used as a residential nonlinear load at PCC. To analyze the various operating conditions, the simulation is carried out in MATLAB. The abnormal grid condition is considered like grid outage and recovery, voltage sag, harmonics in the PCC voltage, and the voltage swell along with analysis due to change in the solar insolation. To show the features of PV-battery system, a wide range of simulated results are presented.

A. Performance at Disappearance of Utility

Fig. 9 presents the response of microgrid at disappearance of utility network. In these scenarios, an OFF signal "0" is delivered to the static switches by the seamless transition algorithm and the phase angle difference is gradually increased. The battery is charged according to the state of change of the battery and the battery voltage is sustained to its prescribed limit in islanded mode. The solar generator supplies the energy to the load and the storage. At fault in the grid, the amplitude, angle, and frequency of the grid voltage are not in the specified limits, and distribution network is separated from the microgrid. An optimum voltage around 240 V is selected and it is boosted to 400 V by using a bidirectional converter. The second harmonic is also mitigated from the BES, which increased the life span of the battery.

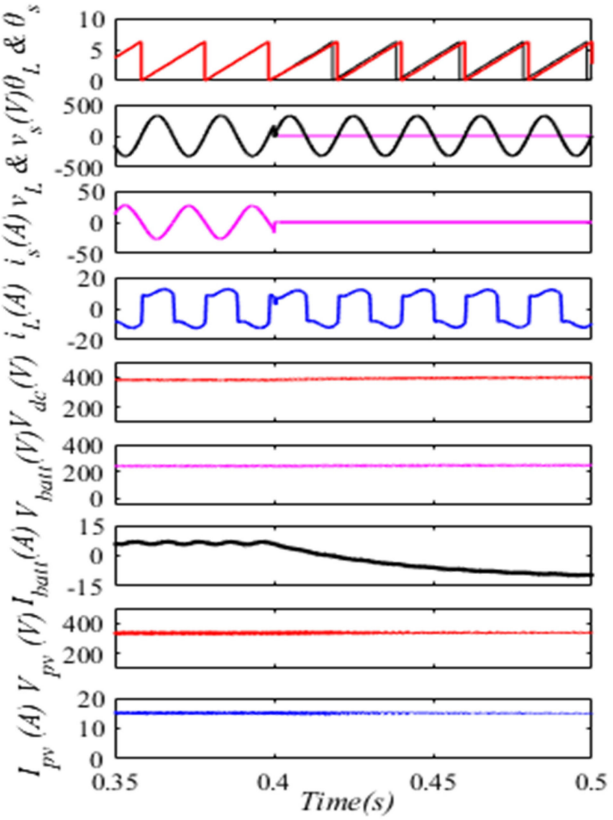

Fig. 9. Simulated behavior of microgrid at sudden outage of grid.

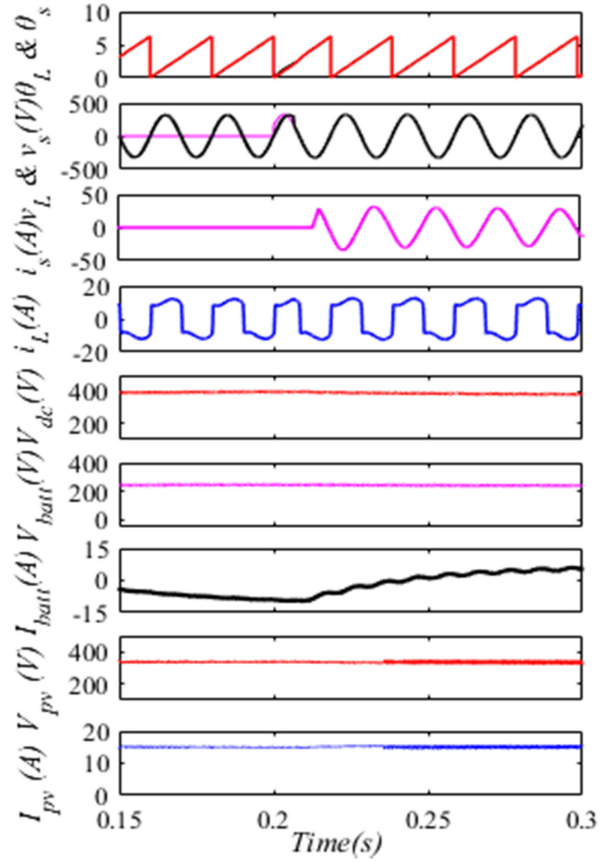

Fig. 10. Simulated behavior of microgrid at sudden recovery of grid.

B. Performance at Sudden Recovery of Grid

Fig. 10 exhibits the simulation results of PV-battery multifunctional system at utility recovery scenarios. The performance is demonstrated in terms of utility and load voltage angles (θ_s and θ_L), grid voltages (v_s) and load voltages (v_L), grid and load voltages (v_s and v_L), grid currents (i_s), load currents (i_L), dc-link voltage ($V_{\rm dc}$), battery voltage ($V_{\rm batt}$) and current ($I_{\rm batt}$), and PV array current and voltage (V_{pv} and I_{pv}). After clearance of fault at 0.2 s, the status of synchronizing turns on the STS and the utility is tied to the VSC. Now, VSC is supervised by the adjustable step-based current control scheme and begins supplying energy to the distribution network. Till 0.2 s, the v_s and i_s are null. After appearance of distribution network, the angle, frequency, and amplitude of v_s, v_L are well matched. The energy across the emergency load is unaltered. The dc-link voltage and battery voltage are maintained to their prescribed values throughout the process.

V. Experimental Results

In the laboratory, the system is implemented. The MPP efficiency under steady-state condition is achieved around 99.8%, which is presented in Fig. 11. This grid-connected PV-battery system consists of solar array simulator (AMETAKE ETS 600/17), which performs the task of a solar PV array. The P–V and I–V characteristics of this solar array simulator are the same as rooftop PV array. The single-phase VSC, a boost converter, RC ripple filter, Hall effect voltage sensors (LV25-P) and current

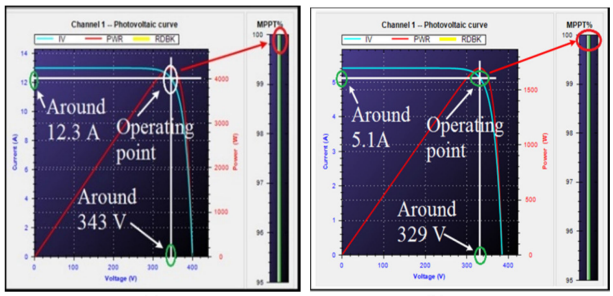

(a) (b)

Fig. 11. MPPT performance (a) at 1000 W/m^2 and (b) at 400 W/m^2.

sensors (LA55-P), nonlinear load at PCC are used. To convert dc solar PV power to ac, VSC is used. Sudden change in the load is created through MCB. In order to provide the isolation and sufficient amount of signal, the opto-couplers are used between the VSC and DSP (dSPACE-1103). All required parameters are sensed and given to a DSP for generating the switching pulses for the boost converter and VSC. An oscilloscope having four channels and power analyzer are used to record test results. The parameters of grid-connected PV-battery system are given in the Appendix.

A. Behavior at Grid Restoration and Outages

Fig. 12(a)–(f) demonstrates behavior of grid interactive multifunctional system at utility restoration and outages conditions.

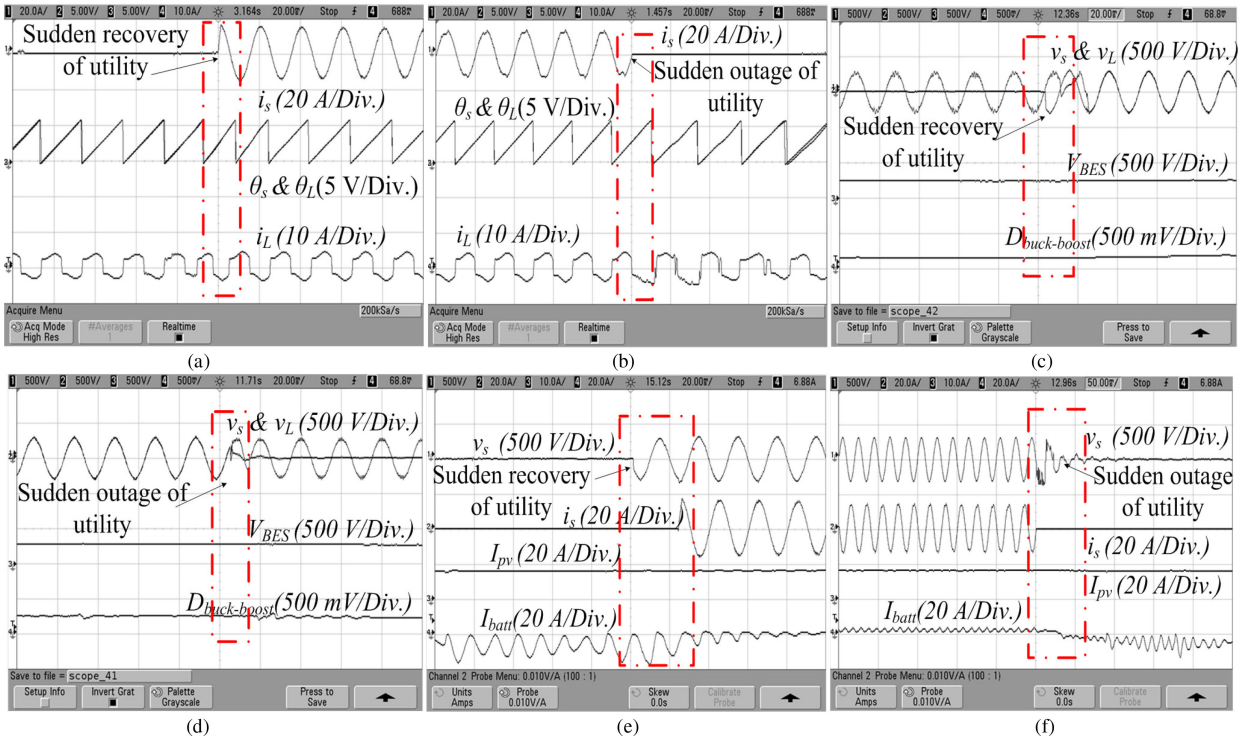

Fig. 12. Experimental results at disappearance and connection of utility.

Fig. 12(a) and (b) presents the utility current (i_s), utility and load voltage angles (θ_s and θ_L), and load current (i_L). The error between the angles is decreased after clearance of the fault and utility grid is recovered. After clearance of fault, angle, frequency, and amplitude of grid and load voltage are observed by the synchronization/islanding technique and provides "1" signal to the switches at appearance of the grid. Furthermore, grid-interactive multifunctional system is supervised using current control technique and starts injecting energy to the utility grid. The load power is uninterrupted throughout the process, islanding to utility-tied mode and vice versa. The utility voltage (v_s), load voltage (v_L), battery voltage ($V_{\rm BES}$), and duty ratio of bidirectional converter are exhibited in Fig. 12(c) and (d). The v_s and v_L are matched as the utility appears. The value of duty ratio is 0.2, which shows the optimum boosting of the BES voltage equal to the dc-link voltage. Fig. 12(e) and (f) presents the v_s, i_s, PV current (I_{pv}), and battery current ($I_{\rm batt}$). After clearance of fault, the energy storage is changed from charging to nonoperating zone and the storage voltage is regulated to its nominal value. After fault occurs, the battery storage is transferred from the floating mode to the charging mode as the solar power is shared between the battery storage and residential load. At all operating conditions, the demand of load is achieved either from renewable source and the grid or from the battery storage. After sudden disappearance of the distribution network, the phase angle difference between the θ_s and θ_L is increased as the grid voltage is not available after the transition and STS is switched from "1" to "0" as the difference in magnitude, phase, and frequency is increased.

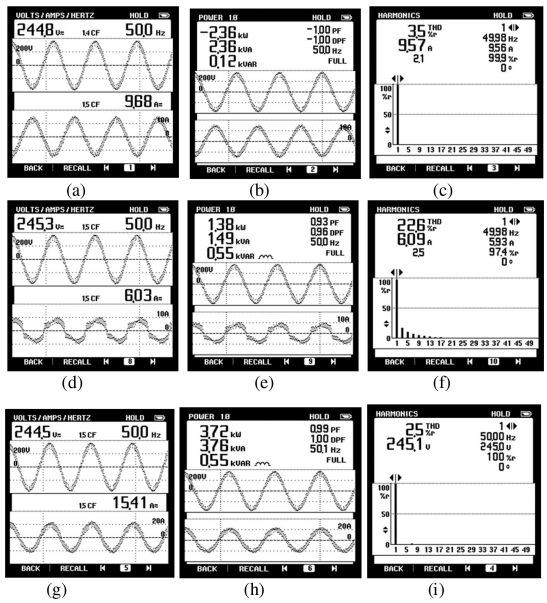

Fig. 13. Experimental results. (a) Utility voltage (v_g) and current (i_g). (b) Utility powers (P_g, Q_g) and power factor. (c) Harmonics graph of i_g, (d) load voltage (v_L), and current (i_L). (e) Load powers (P_L, Q_L). (f) Harmonics graph of i_L, (g) v_g, and VSC currents ($i_{\rm VSC}$). (h) VSC powers. (j) Harmonics graph of v_g.

B. Performance at Nonlinear Load

Fig. 13 presents the experimental performance at nonlinear load. Fig. 13(a)–(c) presents v_g with i_g, utility power (P_g and

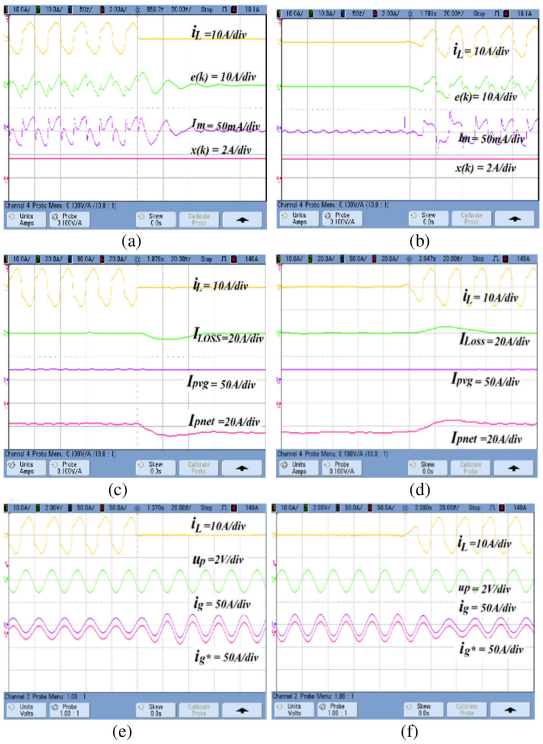

Fig. 14. Intermediate signals of the control algorithm.

Q_g), power factor and harmonics content. The grid current is sinusoidal and harmonics free. Total harmonics distortion (THD) of i_g is presented in Fig. 15(c), which is less than 5%. The load current with load power and harmonics content is shown in Fig. 13(d)–(f). The VSC current, VSC power, and harmonics content of utility voltage are shown in Fig. 13(g)–(i). The extracted power from PV string is sustained by VSC, which is fed to the utility as well as to the load ($2.36 + 1.38 = 3.72$ kW). The negative sign of P_g furnishes that the power is supplied to the distribution network, whereas zero reactive power is supplied to the distribution network at UPF. Moreover, THD and harmonic spectrum of v_g are presented in Fig. 13(i), which follows the criteria of the IEEE 519.

C. Intermediate Signals of Adjustable Step-Based Control

Various intermediate signals of VSC control technique are presented in Fig. 14. In the self-adjustable step-based control, four intermediate signals are presented in Fig. 14(a) and (b). The output of the PI controller, solar participation current, and the peak reference current are presented in Fig. 14(c) and (d). Synchronization signal, sensed grid current, and reference grid current are presented in Fig. 14(e) and (f).

D. Performance at Variation in Irradiance Level

The insolation level of PV array is reduced from 1000 to 400 W/m^2 and the system dynamic behavior is obtained, which is presented in Fig. 15(a) and (b). Because of decrease in PV irradiance level, PV array current is also decreased, while the dc-link voltage remains unchanged. The injected power in the

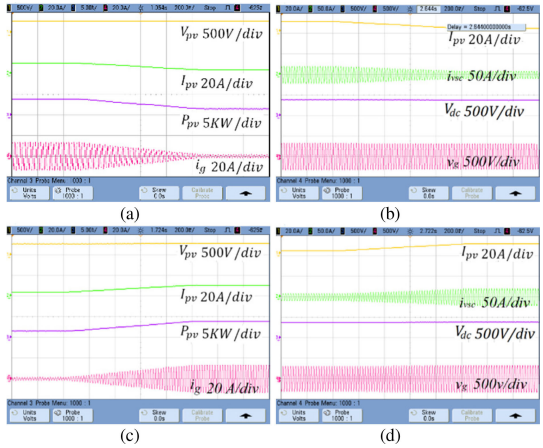

Fig. 15. Behaviour of system at various conditions (1) decrease in insolation. (a) PV array voltage, I_{pv}, P_{pv}, i_g. (b) PV array current, VSC current, dc-link voltage and grid voltage. (2) Increase in insolation. (c) V_{pv}, I_{pv}, PV power, grid current. (d) I_{pv}, VSC current, dc-link voltage, and grid voltage.

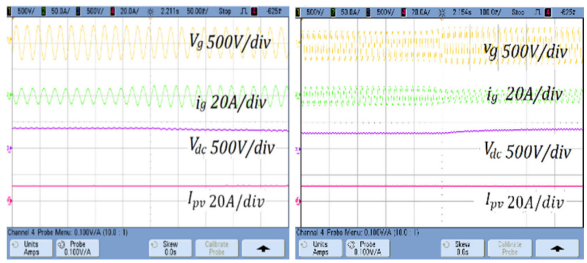

Fig. 16. Salient performance parameters of system under (a) voltage sag and (b) swell conditions, v_g, i_g, $V_{\rm dc}$, and I_{pv}.

grid also decreases, whereas reduction in VSC current is also appeared. Similarly, when insolation level rises from 400 to 1000 W/m^2, PV array current and power are increased. The injection of power in the grid is also increased with VSC current increment, which is demonstrated in Fig. 15(c) and (d).

E. Performance of PV-Battery System at Voltage Sag

When the voltage sag occurs from 240 to 210 V considering nonlinear load at PCC, as shown in Fig. 16(a), the grid current remains sinusoidal because harmonic elimination is performed by the VSC. There is no significant effects in the PV voltage, current, and output power. The dc-link voltage follows the envelope of grid voltage means a decrease in the grid voltage proportionally a decrease in the DC link voltage. This is called adaptive dc-link. However, the converter injects the constant active power at reduced voltage. Therefore, an increase in VSC current is observed. This sag in the voltage is responsible for load current to sag and swell the grid current.

F. Performance of PV-Battery System at Voltage Swell

When the voltage swell occurs from 210 to 253 V considering nonlinear load at PCC, the grid-tied PV inverter response is presented in Fig. 16(b). The grid current remains sinusoidal because harmonic elimination is performed by the VSC but the

nature of the VSC current is nonsinusoidal. Because of voltage swell, there is no significant change in the PV array voltage, current, and PV array output power. The dc-link voltage follows the envelope of grid voltage means an increase in grid voltage proportionally decreases the dc-link voltage. However, the VSC injects constant active energy at increased voltage. Therefore, reduction in converter current is observed. This swell in the voltage is responsible for the load current to be an increase and a decrease in the grid current.

VI. Conclusion

A single-phase two-stage PV-battery system with self-adjustable step-based control algorithm for grid-interactive multifunctional topology has been used for injecting PV energy to the single-phase ac utility and feed the power under outage of the distribution network. This also enhances the quality of current at PCC in grid-interactive mode. A self-adjustable step-based control has been introduced for obtaining the peak load current corresponding to fundamental part. The behavior has been evaluated with extensive changes in working states, consisting of load change, weak utility scenarios, and variation in PV irradiance. This PV-battery system adequately eliminates harmonic component in utility as well as it decreases the losses in line and enhances the voltage waveforms indirectly at PCC. The THD in grid current is reduced under 5% even with nonlinear load (THD $\approx$ 22.6%) PCC, which satisfies the IEEE-519 standard. The PV grid-interactive system performance under steady-state and dynamic conditions has been found satisfactory.

Appendix

System parameters: solar PV array $V_{mpp} = 345$ V, PV array $I_{mpp} = 12.5$ A; solar PV array power 4.3 kW; battery rating, 240 V, 21 Ah; grid voltage 230 V rms and 50 Hz; supply resistance and inductance 0.75 Ω and 2.42 mH, respectively; interfacing inductor = 3.5 mH; ripple filter $R = 6\ \Omega$ and $C = 6\ \mu$F; dc bus capacitor = 5 mF; boost inductor = 5 mH; $K_p = 1$; $K_i = 0.2$; and nonlinear load = 3 kW.

References

[1] Ministry of New and Renewable Energy, Government of India, "Performance analysis of grid connected solar power projects comm. under Phase I of JNNSM, Jan.–Dec. 2014," 2015, pp. 1–4.

[2] A. Askarzadeh and L. Coelho, "A novel framework for optimization of a grid independent hybrid renewable energy system: A case study of Iran," *Solar Energy*, vol. 112, pp. 383–396, Feb. 2015.

[3] P. Kushwaha and C. Bhende, "Single-phase rooftop photovoltaic based grid-interactive electricity system," in *Proc. IEEE Annu. India Conf.*, 2016, pp. 1–6.

[4] N. Kim and B. Parkhideh, "Control and operating range analysis of an AC-stacked PV inverter architecture integrated with a battery," *IEEE Trans. Power Electron.*, vol. 33, no. 12, pp. 10032–10037, Dec. 2018.

[5] H. Trabelsi, "MPPT controllers for PV array panel connected to Grid," in *Proc. 18th Int. Conf. Sci. Techn. Autom. Control Comput. Eng.*, 2017, pp. 505–510.

[6] M. Elgendy, B. Zahawi, and D. Atkinson, "Assessment of the incremental conductance maximum power point tracking algorithm," *IEEE Trans. Sustain. Energy*, vol. 4, no. 1, pp. 108–117, Jan. 2013.

[7] R. John, S. Mohammed, and R. Zachariah, "Variable step size perturb and observe MPPT algorithm for standalone solar photovoltaic system," in *Proc. IEEE Intern. Conf. Intell. Techn. Control Optim. Signal Process.*, 2017, pp. 1–6.

[8] S. Deshpande and N. Bashme, "A review of topologies of inverter for grid connected PV systems," *Innovations Power Adv. Comput. Technol.*, 2017, pp. 1–6.

[9] K. Givaki, D. Chen, and L. Xu, "Current error based compensations for VSC current control in weak grid for wind farm applications," *IEEE Trans. Sustain. Energy*, vol. 10, no. 1, pp. 26–35, Jan. 2019.

[10] C. Jain and B. Singh, "A SOGI-FLL based control algorithm for single phase grid interfaced multifunctional SPV under non-ideal distribution system," in *Proc. Annu. IEEE India Conf.*, 2014, pp. 1–6.

[11] H. Li, Y. Huang, and J. Lu, "Reactive power compensation and DC link voltage control using fuzzy-PI on grid-connected PV system with D-STATCOM," in *Proc. IEEE PES Asia-Pacific Power Energy Eng. Conf.*, 2016, pp. 1240–1244.

[12] S. Kumar and B. Singh, "A multipurpose PV system integrated to a three-phase distribution system using an LWDF-based approach," *IEEE Trans. Power Electron.*, vol. 33, no. 1, pp. 739–748, Jan. 2018.

[13] S. Kumar and B. Singh, "Implementation of high-precision quadrature control for single-stage SECS," *IEEE Trans. Ind. Inform.*, vol. 13, no. 5, pp. 2726–2734, Oct. 2017.

[14] Z. Yao, L. Xiao, and Y. Yan, "Seamless transfer of single-phase grid interactive inverters between grid-connected and stand-alone modes," *IEEE Trans. Power Electron.*, vol. 25, no. 6, pp. 1597–1603, Jun. 2010.

[15] B. Singh, A. Chandra, and K. Al-Haddad, *Power Quality: Problems and Mitigation Techniques*. India: Wiley-Blackwell, Jan. 2015.

[16] *IEEE Standard for Interconnection and Interoperability of Distributed Energy Resources with Associated Electric Power Systems Interfaces*, IEEE Std 1547-2018 (Revision of IEEE Std 1547-2003), p. 1138, Apr. 2018.

[17] C. Zhang, X. Zhao, X. Wang, X. Chai, Z. Zhang, and X. Guo, "A grid synchronization PLL method based on mixed second- and third-order generalized integrator for DC offset elimination and frequency adaptability," *IEEE J. Emerg. Sel. Topics Power Electron.*, vol. 6, no. 3, pp. 1517–1526, Sep. 2018.

[18] C. Subramanian and R. Kanagaraj, "Rapid tracking of grid variables using prefiltered synchronous reference frame PLL," *IEEE Trans. Instrum. Measur.*, vol. 64, no. 7, pp. 1826–1836, Jul. 2015.

[19] T. Youssef and O. Mohammed, "Adaptive SRF-PLL with reconfigurable controller for microgrid in grid-connected and stand-alone modes," in *Proc. IEEE Power Energy Soc. General Meeting*, 2013, pp. 1–5.

[20] M. Ghartemani, S. Khajehoddin, P. Jain, and A. Bakhshai, "Problems of startup and phase jumps in PLL systems," *IEEE Trans. Power Electron.* vol. 27, no. 4, pp. 1830–1838, Apr. 2012.

[21] R. Chilipi, N. Sayari, K. Hosani, M. Fasil, and A. Beig, "Third order sinusoidal integrator (TOSSI)- control algorithm for shunt active power filter under distorted and unbalanced voltage conditions," *Int. J. Elect. Power Energy Syst.*, vol. 96, pp. 152–162, 2018.

[22] D. Mlakić, S. Nikolovski, and H. Baghaee, "Hybrid method for islanding detection of distributed generators in LV distribution networks," in *Proc. 18th IEEE Int. Conf. Smart Technol.*, 2019, pp. 1–6.

[23] A. Abokhalil, A. Awan, and A. Al-Qawasmi, "Comparative study of passive and active islanding detection methods for PV grid-connected systems," *MDPI*, vol. 10, pp. 1–15, May 2018.

[24] H. Li, Z. Wu, and F. Lui, "A novel variable step size adaptive harmonic detecting algorithm applied to active power filter," in *Proc. IEEE Int. Conf. Ind. Technol.*, 2016, pp. 574–578.

[25] L. Patel, S. Kumar, B. Singh, and A. Vyas, "Self-adjustable step based control algorithm for multifunctional PV system under sag-swell conditions," in *Proc. IEEE Int. Conf. Power Electron. Drives Energy Syst.*, Chennai, India, 2018, pp. 1–6.

Shailendra Kumar (Member, IEEE) was born in Mahoba, India, in 1988. He received the M.Tech. degree in power electronics, from IIT, Delhi, India, in 2015. He received the Ph.D. degree from the Department of Electrical Engineering, IIT Delhi, in 2019.

Currently, he is working as an Assistant Professor with the Department of Electrical Engineering, SVNIT, Surat, India. His research interests include power quality, grid integration, and microgrid.

Dr. Kumar received POSOCO Power System Award (in Master and Doctoral categories) in 2016 and 2019. He is also a recipient of Prof. Som Nath Mahendra Student Travel Awards for the IEEE PEDES 2018 conference and the IEEE UPCON Best Paper Award in 2016 and 2018.

Laxmi Narayan Patel was born in Latesara, India, in 1989. He received the B.Tech. degree in electrical and electronics engineering from the Bhilai Institute of Technology, Durg, India, in 2013, and the M.Tech. degree in instrument technology from the Indian Institute of Technology, Delhi, India, in 2018.

Currently, he is working as a Senior Application Engineer with Applied Materials, Bengaluru, India. His research interests include power electronics, drives, power quality, grid-interfaced solar photovoltaic systems, and design of custom power devices.

Bhim Singh (Fellow, IEEE) was born in Rahamapur, Bijnor (UP), India, in 1956. He received the B.E. (electrical) degree from the University of Roorkee (now IIT Roorkee), India, in 1977, and the M.Tech. (power apparatus and systems) and Ph.D. degrees in electrical engineering from the Indian Institute of Technology Delhi, India, in 1979 and 1983, respectively.

In 1983, he joined the Department of Electrical Engineering, University of Roorkee, as a Lecturer. He became a Reader there in 1988. In December 1990, he joined the Department of Electrical Engineering, IIT Delhi, India, as an Assistant Professor, where he has become an Associate Professor in 1994 and a Professor in 1997. He has been the Head of the Department of Electrical Engineering, IIT Delhi, from July 2014 to August 2016. Since August 2016, he has been the Dean, Academics, IIT Delhi. He has guided 83 Ph.D. dissertations, and 167 M.E./M.Tech./M.S.(R) theses. He holds 52 patents. He has executed more than 80 sponsored and consultancy projects. His research interests include solar PV grid interface systems, microgrids, power quality monitoring and mitigation, solar PV water pumping systems, improved power quality ac–dc converters, power electronics, electrical machines, drives, flexible alternating transmission systems, and high-voltage direct current systems.

Dr. Singh has been a JC Bose Fellow of DST, Government of India since December 2015. He has also been CEA Chair Professor since January 2019.

Anoop Lal Vyas received the B.Tech. degree in electrical engineering in 1972 and the Ph.D. degree in 1989, both from IIT Delhi, India.

Since 1972, he has been working in the areas of sonar signal processing, underwater electronics, and electronic systems, and has coordinated a number of projects in these areas. His research interests include electronic instrumentation, smart sensors, body area networks, health monitoring, and standalone power systems.

Dr. Vyas, presently, holds the position of Emiretus Professor in Instrument Design Development Centre, IIT Delhi.